

# Approximate Analytical Solution to Diurnal Atmospheric Boundary-Layer Growth Under Well-Watered Conditions

J. R. Rigby<sup>1</sup> · Jun Yin<sup>2</sup> · John D. Albertson<sup>2</sup> · Amilcare Porporato<sup>2</sup>

Received: 22 September 2014 / Accepted: 5 March 2015 / Published online: 31 March 2015  
© Springer Science+Business Media Dordrecht (outside the USA) 2015

**Abstract** Simplified numerical models of the atmospheric boundary layer (ABL) are useful both for understanding the underlying dynamics and potentially providing parsimonious modelling approaches for inclusion in larger models. Herein the governing equations of a simplified slab model of the uniformly mixed, purely convective, diurnal ABL are shown to allow immediate solutions for the potential temperature and specific humidity as functions of the ABL height and net radiation when expressed in integral form. By employing a linearized saturation vapour relation, the height of the mixed layer is shown to obey a non-linear ordinary differential equation with quadratic dependence on ABL height. A perturbation solution provides general analytical approximations, of which the leading term is shown to represent the contribution under equilibrium evaporation. These solutions allow the diurnal evolution of the height, potential temperature, and specific humidity (i.e., also vapour pressure deficit) of the mixed layer to be expressed analytically for arbitrary radiative forcing functions.

**Keywords** Analytical solution · Atmospheric boundary layer · Bowen ratio · Equilibrium evaporation · Evaporative fraction · Mixed-layer model · Perturbation theory

---

✉ J. R. Rigby  
jr.rigby@ars.usda.gov

Jun Yin  
jun.yin@duke.edu

John D. Albertson  
john.albertson@duke.edu

Amilcare Porporato  
amilcare@duke.edu

<sup>1</sup> USDA-ARS National Sedimentation Laboratory, Oxford, MS 38655, USA

<sup>2</sup> Department of Civil and Environmental Engineering, Duke University, Durham, NC 27708, USA

## 1 Introduction

The daytime (diurnal) atmospheric boundary layer (ABL) is the turbulent mixing region below the relatively stable free atmosphere. The turbulence in the ABL is principally maintained by shear-driven and buoyancy-driven convection. Within the middle portion of this region, the temperature profiles are nearly adiabatic, while the specific humidity tends to slightly decrease with height due to the moisturizing effects from below and the drying process from above (Mahrt 1976; Stull 1988; Garratt 1994). The top of this mixed layer is capped by a rapid change in potential temperature, the so-called capping inversion, where the vertical profile reverts to (stable) free atmospheric conditions. The physical characteristics of this mixing region are controlled by both surface and free atmospheric conditions and in turn govern the vertical heat and mass transport between land surface and atmosphere.

Simplified slab models of the ABL were first developed in the late 1960s and early 1970s as in, e.g., Ball (1960), Lilly (1968), Tennekes (1973), Carson (1973), Betts (1973), and subsequently by many others (e.g., Driedonks 1982b; McNaughton and Spriggs 1986; Raupach 1998, 2000, 2001). More recently, Porporato (2009) investigated a simplified purely convective ABL slab model with the added assumption of a constant daytime Bowen ratio, an approximation supported for midday conditions by Brutsaert (1987) on daytime evaporative fractions. Despite their zero-dimensional simplification, mixed-layer models agree favorably with observations and results from large-eddy simulation (Betts 1992; Kim and Entekhabi 1998; Pelly and Belcher 2001). When coupled to mass and heat transfer between the land surface and the atmosphere, mixed-layer models provide an efficient benchmark for a wide range of applications, from atmospheric pollutant transport to the understanding of eco-hydrological dynamics to parametrization schemes for large-scale climate models (McNaughton and Spriggs 1986; Kim and Entekhabi 1998; Lyons 2002; Juang et al. 2007; Siqueira et al. 2009; Konings et al. 2010).

However, in the presence of evapotranspiration even the simplest zero-dimensional mixed-layer model does not permit analytical solutions, thus complicating any potential analysis and physical interpretation of the land-atmosphere interaction. To progress in this direction, we discuss approximate analytical solutions for the mixed-layer model in the coupled land-atmosphere system. As a first attempt, we confine our study to well-watered conditions, under which the stomatal conductance and aerodynamic conductance are assumed to be constant. In Sect. 2 we show immediate solutions for the potential temperature and specific humidity in terms of the ABL height. In Sect. 3, we employ a linearized saturation vapour curve, which allows us to solve for the surface-layer temperature, providing an approximate solution to the surface energy balance. Using this solution for the surface energy balance we derive a non-linear differential equation governing the evolution of the ABL height under equilibrium evaporation in Sect. 4. Analytical solutions for specific forcings are developed in Sect. 5 which result in an Abel equation of the second kind and simplifications thereof. In Sect. 6, we use perturbation methods to find the analytical approximation for arbitrary forcing, and in Sect. 7 we revisit the constant Bowen ratio solution of Porporato (2009) to derive the effective Bowen ratio for use in that case. In Sect. 8 we test our models and compare the various solutions with observations from the Central Facility, Southern Great Plains (CF-SGP). Finally, conclusions are summarized in Sect. 9.

## 2 Basic Equations of the Diurnal Convective ABL Over Land (Models M0 and M1)

At the surface, energy flux partitioning is controlled by the surface energy balance given in simplified form as

$$Q(t) = R_{\text{net}}(t) - G(t) = H(t) + \lambda E(t), \tag{1}$$

where  $t$  is time,  $Q$  is the net available energy,  $R_{\text{net}}$  is the net radiation at the surface,  $G$  is the ground heat flux,  $H$  is the sensible heat flux,  $\lambda$  is the specific latent heat of vaporization, and  $E$  is the evaporative flux. The latter two energy fluxes can be expressed as

$$H(t) = g_h c_p \rho [\theta_s(t) - \theta(t)], \tag{2a}$$

$$E(t) = g_e \rho [q_s^*(t) - q(t)], \tag{2b}$$

where  $\rho$  is the density of air,  $c_p$  is the heat capacity at constant pressure,  $q^*$  is the saturation specific humidity,  $q$  is the specific humidity in the mixed layer,  $\theta$  is the potential temperature in the mixed layer, and  $g_e$  and  $g_h$  are the conductances to water vapour and sensible heat transfer. The subscript  $s$  refers to the values at the surface. When no subscript is given the variable is understood to represent conditions within the mixed layer. The conductances  $g_h$  and  $g_e$  typically consist of a series of canopy and atmospheric conductances,

$$g_h = 1/r_a, \tag{3a}$$

$$g_e = 1/(r_a + r_s), \tag{3b}$$

where  $r_a$  is aerodynamic resistance and  $r_s$  is surface resistance. The surface resistance describes the resistance of water flow through the crop and soil surface. The aerodynamic resistance, which is stability dependent, controls the transfer of heat and water from the evaporating surface into the air above the canopy. Under well-watered and stationary conditions (assumed herein), the two conductances  $g_h$  and  $g_e$  may be assumed to be constant.

The conservation of dry static energy in the mixed layer gives,

$$\rho c_p h \frac{d\theta}{dt} = H(t) + \rho c_p [\theta_f(h) - \theta] \frac{dh}{dt}, \tag{4}$$

and similarly, the conservation of the mass of water vapour in the mixed layer yields,

$$\rho h \frac{dq}{dt} = E(t) + \rho [q_f(h) - q] \frac{dh}{dt}. \tag{5}$$

Here the subscript  $f$  refers to the values of the free atmospheric profiles. To close these equations, the buoyancy flux at the top of the boundary layer is often assumed to be related to the surface buoyancy flux (contribution from convection turbulence) and surface shear stress (contribution from mechanical turbulence) (Driedonks 1982a; Batchvarova and Gryning 1991, 1994). To study the essential processes of heat-flux partitioning in the land-atmosphere interaction, we focus on the warm seasons when buoyancy-driven turbulence dominates the convection and mechanical turbulence becomes negligible. To further simplify the entrainment and make the system analytically solvable, we use sensible heat flux ( $w'\theta'$ ) to approximate the buoyancy flux ( $\overline{w'\theta'_v}$ ) and model the entrainment as (Stull 1988; Garratt 1994),

$$[\theta_f(h) - \theta] \frac{dh}{dt} = -(\overline{w'\theta'})_h = \beta(\overline{w'\theta'})_s, \tag{6}$$

which is tested later with observations. The model using the buoyancy flux ( $\overline{w'\theta'_v}$ ) is referred to as M0 and the model using the sensible heat flux ( $\overline{w'\theta'}$ ) without considering humidity effects

on buoyancy is referred to as M1. A comparison between these two models is discussed in Sect. 8. The ratio  $\beta$  ranges from 0.1 to unity with a typical value of 0.2 (Ball 1960; Stull 1976; Seibert et al. 2000); Angevine (2008) and Canut et al. (2012) recently summarized the uncertainties of  $\beta$  based on observations and large-eddy simulations.

Following the common modelling assumptions of linear free atmospheric profiles (e.g., Tennekes 1973; Porporato 2009),

$$\theta_f(z) = \gamma_\theta z + \theta_{f0}, \quad (7a)$$

$$q_f(z) = \gamma_q z + q_{f0}, \quad (7b)$$

where  $\gamma_\theta$  and  $\gamma_q$  are the slopes of free atmospheric potential temperature and specific humidity and are treated as constant, the growth of the simplified diurnal boundary layer can be modelled as (Tennekes 1973; Garratt 1994),

$$\frac{dh}{dt} = \frac{(1 + 2\beta)H(t)}{\rho c_p \gamma_\theta h}. \quad (8)$$

Once the surface and free atmospheric conditions and the radiative forcing are specified, Eqs. 1–8 in conjunction with the Clausius–Clapeyron relation represent a closed system of coupled, non-linear differential-algebraic equations for the idealized diurnal mixed layer. The system can be solved numerically but presents challenges analytically due to its strong coupling and non-linearity. Analytical solutions are desirable, however, both to provide insight into the dynamical relationships of the state variables and potentially for use in parametrizing boundary-layer dynamics in large-scale models.

To further understand this system, it is important to first analyze the components that contribute to the growth of the boundary layer. Rewriting Eq. 2b by separating the contribution from saturation differences at the surface and the air, and the contribution from saturation deficit in the air, as typically done in the Penman–Monteith or combination approach (Rau-pach 2001; Brutsaert 2005), one obtains,

$$E = g_e \rho (q_s^* - q^* + q^* - q) = g_e \rho (q_s^* - q^*) + g_e \rho (q^* - q), \quad (9)$$

where the first component is the equilibrium evaporation and the second component is the evaporative flux due to vapour pressure deficit (i.e. the so-called drying power of the air),

$$E_{eq} = g_e \rho (q_s^* - q^*), \quad (10a)$$

$$E_{vpd} = g_e \rho (q^* - q). \quad (10b)$$

Combining Eqs. 9–10 and Eq. 1 and substituting into Eq. 8 yields,

$$\frac{dh}{dt} = \frac{1 + 2\beta}{\rho c_p \gamma_\theta h} [Q - \lambda(E_{eq} + E_{vpd})]. \quad (11)$$

The boundary-layer growth is controlled by  $\lambda E_{eq}$  and  $\lambda E_{vpd}$ , while, through the definition of Bowen ratio,

$$Bo = \frac{H}{\lambda E} = \frac{H}{Q - H}, \quad (12)$$

the growth of the ABL can also be rewritten as,

$$\frac{dh}{dt} = \frac{1 + 2\beta}{\rho c_p \gamma_\theta h} \left[ \frac{Bo}{1 + Bo} Q(t) \right]. \quad (13)$$

The growth of the boundary layer expressed by Eq. 13 indicates that the Bowen ratio may be further separated into components due to equilibrium evaporation and vapour pressure deficit

as in Eq. 11, a point that is investigated in later sections. Note that one could also express the surface energy partitioning using the evaporative fraction (Brutsaert 2005).

Following Porporato (2009) we introduce the change of variable,

$$\tilde{\theta} = \theta - \theta_{f0}, \tag{14a}$$

$$\tilde{q} = q - q_{f0}. \tag{14b}$$

Employing this change of variable, Eqs. 4 and 8 can be combined to form a pair of exact differential equations, which can be integrated analytically to find  $\tilde{\theta}$  as a function of mixed-layer height,

$$\tilde{\theta} = \gamma_{\theta} \frac{1 + \beta}{1 + 2\beta} h, \tag{15}$$

where the initial condition  $\tilde{\theta}(t = 0) = 0$  implies that the constant of integration vanishes (Garratt 1994; Porporato 2009). Similarly, we can combine Eqs. 5 and 8 with the total energy balance,  $Q = \lambda E + H$ , and integrate to find an expression for  $\tilde{q}$  in terms of  $h$  and  $t$ ,

$$\tilde{q} = \frac{1}{\lambda \rho h(t)} \int_0^t Q(u) du + \frac{1}{2} \left( \gamma_q - \frac{c_p \gamma_{\theta}}{\lambda(1 + 2\beta)} \right) h(t), \tag{16}$$

where  $\tilde{q}(t)$  is a function of ABL height  $h(t)$  and time  $t$ .

Thus, the specific humidity and potential temperature are known analytically if the integrated net available energy and the height of the boundary layer are given. Substituting these into Eqs. 10 and 11 gives

$$\frac{dh}{dt} = \frac{(1 + 2\beta)}{\rho c_p \gamma_{\theta} h} \left\{ Q(t) - \rho \lambda g_e \left[ q^*(\theta_s) - \frac{1}{\lambda \rho h(t)} \int_0^t Q(u) du + \frac{h(t)}{2} \left( \gamma_q - \frac{c_p \gamma_{\theta}}{\lambda(1 + 2\beta)} \right) \right] \right\}, \tag{17}$$

demonstrating that the only remaining hurdle to having a single equation for the diurnal growth of the mixed layer is the surface energy balance, neatly represented here by  $q^*(\theta_s)$ .

### 3 Linearization of the Saturated Vapour Pressure Curve (Model M2)

Combining the surface flux equations and the total energy balance yields

$$Q = \lambda g_e \rho (q_s^* - q) + \rho g_h c_p (\theta_s - \theta). \tag{18}$$

If we now make the change of variables,

$$\tilde{q}_s^* = q^*(\theta_s) - q^*(\theta_{f0}), \tag{19a}$$

$$\tilde{\theta}_s = \theta_s - \theta_{f0}, \tag{19b}$$

we have

$$\frac{Q}{\rho} = \lambda g_e (\tilde{q}_s^* - \tilde{q}) + \lambda g_e (q_{\theta_{f0}}^* - q_{f0}) + g_h c_p (\tilde{\theta}_s - \tilde{\theta}), \tag{20}$$

and we note that the second term represents the initial saturation specific humidity deficit,  $\Delta_{q0}$ , a constant. Equation 20 describes the surface energy balance in our simplified system, where the surface temperature,  $\theta_s$ , appears twice in this equation: once as an argument to the saturation specific humidity function,  $q_s^* = q^*(\theta_s)$ , and once explicitly. Attempting to solve this equation for  $\theta_s$  yields,

$$\tilde{q}^*(\theta_s) + \frac{g_h c_p}{\lambda g_e} \tilde{\theta}_s = \frac{Q}{\rho \lambda g_e} + \tilde{q} + \frac{g_h c_p}{\lambda g_e} \tilde{\theta} - \Delta q_0, \tag{21}$$

which provides an implicit solution but does not solve the problem in Eq. 17.

To surmount this difficulty, we again follow the Penman-Monteith or combination approach (Raupach 2001; Brutsaert 2005) to linearize the saturation specific humidity curve by expanding in a Taylor series to first order around a suitable reference temperature and assign the slope at the reference temperature to be the constant  $\epsilon_r$ . The reference temperature, representing the typical temperature of the day, could be chosen as the temperature close to the expected midday values of  $\theta$ . This provides a first-order approximate saturation specific humidity relation,

$$\tilde{q}_s^* \approx \epsilon_r(\theta_s - \theta_{f_0}) = \epsilon_r \tilde{\theta}_s \tag{22}$$

with which we can find the equilibrium Bowen ratio as the ratio of sensible heat flux, Eq. 2a, to the equilibrium evaporation, Eq. 10a (Priestley and Taylor 1972; McNaughton 1976; De Bruin 1983; Garratt 1994; Betts 1994; Culf 1994; Heerwaarden et al. 2009),

$$Bo_{eq} = \frac{H}{\lambda E_{eq}} = \frac{g_h c_p \rho (\theta_s - \theta)}{\lambda g_e \rho (q_s^* - q^*)} = \frac{g_h c_p}{\lambda g_e \epsilon_r}. \tag{23}$$

This equilibrium Bowen ratio is also the upper limit of the Bowen ratio as  $Q \rightarrow \infty$ . Generally, when keeping all other variables fixed, the Bowen ratio increases with the increasing available energy ( $Q$ ) and quickly reaches an upper limit ( $Bo_{eq} = Bo_{max}$ ) (see Porporato 2009, Fig. 5).

Substituting Eqs. 22 and 23 into the surface energy balance, Eq. 20, gives an approximate surface temperature,

$$\tilde{\theta}_s \approx \frac{Bo_{eq}}{1 + Bo_{eq}} \left( \frac{Q}{\rho g_h c_p} + \frac{\lambda g_e}{c_p g_h} \tilde{q} + \tilde{\theta} - \frac{\lambda g_e \Delta q_0}{g_h c_p} \right). \tag{24}$$

This approximate solution for  $\tilde{\theta}_s$  is conveniently linear and separable in  $Q$ ,  $\tilde{\theta}$ , and  $\tilde{q}$ . Substituting Eqs. 15 and 16 into Eq. 24 yields the desired representation of  $\tilde{\theta}_s$  as a function of  $h$  and  $t$  only, which greatly simplifies the surface coupling for the sake of analytical treatment.

Substituting  $\tilde{\theta}_s$  from Eq. 24 into the combination of Eqs. 1, 2a, and 8 gives the following non-linear ordinary differential equation (model M2),

$$\underbrace{\frac{dh}{dt}}_I = \underbrace{\frac{f(t)}{h}}_II + \underbrace{\frac{g(t)}{h^2}}_III + \underbrace{C}_{IV}, \tag{25}$$

where,

$$f(t) = \frac{1 + 2\beta}{\rho c_p \gamma_\theta} \frac{Bo_{eq}}{1 + Bo_{eq}} (Q(t) - \rho \lambda g_e \Delta q_0), \tag{26a}$$

$$g(t) = g_e \frac{1 + 2\beta}{\rho c_p \gamma_\theta} \frac{Bo_{eq}}{1 + Bo_{eq}} \int_0^t Q(u) du, \tag{26b}$$

$$C = \left( -\frac{1 + \beta}{1 + Bo_{eq}} \right) g_h + \left( -\frac{c_p \gamma_\theta - \lambda \gamma_q (1 + 2\beta)}{2 c_p \gamma_\theta} \frac{Bo_{eq}}{1 + Bo_{eq}} \right) g_e. \tag{26c}$$

Note that the constant  $C$  is a linear combination of  $g_h$  and  $g_e$  with coefficients depending primarily on the atmospheric lapse rates and equilibrium Bowen ratio ( $Bo_{eq}$ ). Equation 26c also suggests  $C$  is negative when  $\gamma_\theta$  is positive and  $\gamma_q$  is negative, which is usually true above a well-watered surface.

Thus, we have shown that the system of equations for  $h$ ,  $\theta$ , and  $q$  can be reduced exactly to the single problem of solving the coupling of the surface energy balance with the ABL height,  $h$ . Further, linearizing the saturation vapour pressure curve provides a non-linear first-order ordinary differential equation for the ABL height, the solution to which solves the entire model approximately. Equation 25 still resists analytical solution, however, due to its strong non-linearity. In the sections to follow we consider this equation and its approximate solutions in more detail.

### 4 Equilibrium Solution (Model M3)

While Eq. 25 is unlikely to yield a closed-form solution, we can make a “first guess” at a solution by considering the case under equilibrium evaporation, i.e., when the terms  $g(t)/h^2 + C$  are very small or cancel one another resulting in an exactly solvable condition. In such a case, Eq. 25 reduces to

$$\frac{dh}{dt} = \frac{f(t)}{h}. \tag{27}$$

Assuming no morning transient ( $h(0) = 0$ ) and no initial humidity deficit under well-watered conditions ( $\Delta_{q_0} = 0$ ), then we have the solution

$$h_{eq}(t) = \left( 2 \int_0^t f(u) du \right)^{1/2}. \tag{28}$$

This “equilibrium” solution has exactly the same form of the solution for the mixed layer under constant Bowen ratio as in Tennekes (1973), Garratt (1994), and Porporato (2009). In this case, the constant Bowen ratio becomes the Bowen ratio under equilibrium evaporation ( $Bo = Bo_{eq}$ ), which is the algebraic limit of the Bowen ratio as  $Q \rightarrow \infty$  (Porporato 2009). Due to the overestimation of the Bowen ratio, the equilibrium solution also overestimates the rate of boundary-layer growth. Figure 1 (left) compares the numerical solution to Eq. 25 (M2) with the equilibrium solution  $h_{eq}(t)$  (M3). Though overestimating the mixed-layer

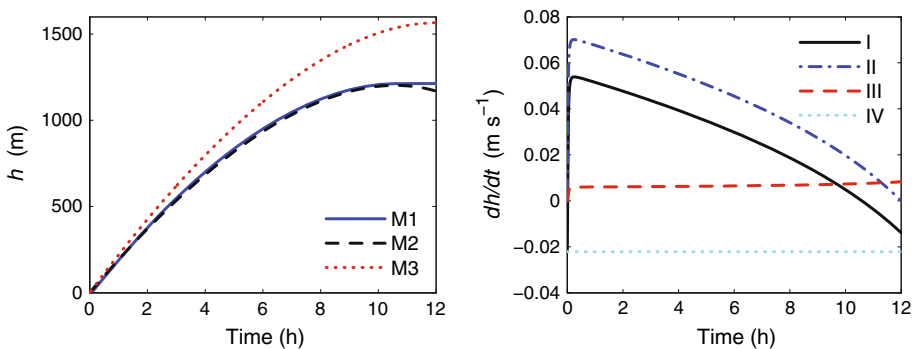


**Fig. 1** *Left* numerical solution for the ABL height from full numerical simulation (M1), linearized saturation vapour pressure curve approximation (M2), and constant equilibrium Bowen ratio model (M3) (see Table 1 for a detailed model description). *Right* numerical simulation of the mixed-layer height growth rate of each individual term in Eq. 25. The parameters in these numerical solutions and simulations represent typical surface and atmospheric characteristics in warm seasons under well-watered condition (see Table 2)

height through much of the day, the shape of the equilibrium solution is consistent with the fully non-linear version and thus encourages further analysis to find a good approximation.

## 5 Approximation to an Abel Equation

Looking closer at the system, Fig. 1 (right) shows each term in Eq. 25 solved numerically. As can be seen, terms I and II are almost parallel to each other with a distance related to the sum of terms III and IV. During the diurnal evolution, term III does not show any noticeable variation and term IV is constant as defined in Eq. 26c.

The behaviour of term III suggests that substituting a constant in its place would be a reasonable approximation. Recalling that  $g(t) = g_e \int f(t)dt$ , we can rewrite term III as,

$$\frac{g(t)}{h^2} = \frac{g_e}{2} \left( \frac{h_{\text{eq}}(t)}{h} \right)^2. \quad (29)$$

In this form, as  $h_{\text{eq}}/h \rightarrow 1$ , the term in brackets approaches  $g_e/2$ . and the sum of terms III and IV in Eq. 25 approaches  $g_e/2 + C$ . Since  $C$  in Eq. 26c is generally negative in value, and  $h_{\text{eq}}$  is larger than  $h$ , we can expect the sum of terms III and IV to approach zero “from the right” so that in general  $g_e/2 + C \leq (\text{III}+\text{IV}) < 0$ . Assuming a correction factor that equally splits the difference of this interval, the sum of terms III and IV may be approximated as,

$$\begin{aligned} C' &= \frac{1}{2} \left( C + \frac{g_e}{2} \right) \\ &= \left( -\frac{1 + \beta}{2(1 + B_{\text{oeq}})} \right) g_h + \left( \frac{c_p \gamma_\theta + \lambda \gamma_q B_{\text{oeq}}(1 + 2\beta)}{4c_p \gamma_\theta (1 + B_{\text{oeq}})} \right) g_e. \end{aligned} \quad (30)$$

Similar to  $C$ ,  $C'$  is again another linear combination of  $g_h$  and  $g_e$ , and with this approximation, Eq. 25 becomes

$$\frac{dh}{dt} = \frac{f(t)}{h} + C'. \quad (31)$$

From a physical point of view,  $f(t)/h$  in Eq. 31 contributes to the ABL growth through the equilibrium evaporation ( $E_{\text{eq}}$ ), while the  $C'$  in (31) influences the ABL growth by the evaporation through the vapour pressure deficit ( $E_{\text{vpd}}$ ). From a mathematical point of view, Eq. 31 is a particular form of Abel’s equation of the second kind, which is itself a generalization of the Riccati equation (Zaitsev and Polyinin 2012). We can set the equation to a normal form by introducing the change of variable  $y = h(t)/C'$ ,

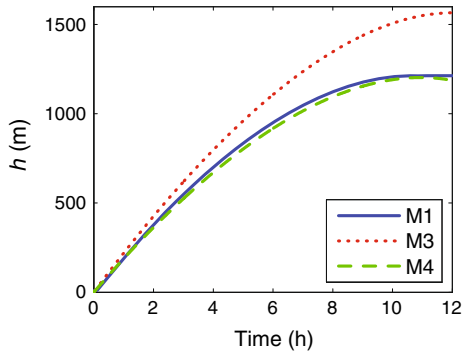
$$yy'_t - y = F(t), \quad (32)$$

where  $F(t) = f(t)/C'^2$  and represents a rescaled radiative forcing function. Unfortunately no general solution exists for this Abel equation for arbitrary forcing  $F(t)$ . Closed-form solutions of the Abel equation for specific forcing functions (see Zaitsev and Polyinin 2012) will be explored in subsequent contributions, while here we proceed seeking further approximations of sufficiently general validity.

## 6 Solution with an Effective Bowen Ratio (Model M4)

As Eq. 31 cannot be solved directly for an arbitrary forcing function, a perturbation method (Logan 2013) is used here to find the approximation solution. By assuming  $C'$  is a small term

**Fig. 2** The mixed-layer height as a function of time predicted by the full numerical simulation (M1), constant equilibrium Bowen ratio model (M3), and the approximate solution  $\bar{h}(t)$  (M4) (see Table 1 for detailed description of models). The parameters for simulations can be found in Table 2



and writing the solution  $h(t)$  in perturbation series to the first order as  $h(t) = h_0(t) + C'h_1(t)$ , we can find that  $h_0(t) = h_{eq}(t)$  and  $h_1(t) = t$  and thus the first-order approximation is given as,

$$\bar{h}(t) = h_{eq}(t) + C't. \tag{33}$$

Clearly, the first term on the right-hand side ( $h_{eq}$ ) is the equilibrium solution and the second term ( $C't$ ) is the perturbation term, accounting for the contribution from evaporation due to vapour pressure deficit. This model is referred to as M4 hereafter. As shown in Fig. 2, this approximation works well (see Sect. 8 below for a more comprehensive test of the models). The inclusion of  $C'$  in M4 adds the contribution from the vapour pressure deficit that efficiently reduces the resulting overestimation from the equilibrium solution of M3.

Having an analytical solution for the height of the ABL provides an approximate solution to the entire system (i.e., for  $h, \theta$ , and  $q$ ) since  $q$  and  $\theta$  can be expressed exactly as functions of the ABL height and time (Eqs. 15 and 16). The resulting approximate solutions are discussed below.

The daytime evolution of the potential temperature in the mixed layer is found by substituting  $\bar{h}$  from Eq. 33 into the relation for  $\theta$ , Eq. 15. Similarly, the daytime evolution of the specific humidity is found by substituting the approximate ABL height into Eq. 16. The resulting approximate analytical results (M4) are plotted alongside full numerical simulation (M1) as well as the constant equilibrium Bowen ratio solution (M3) in Fig. 3.

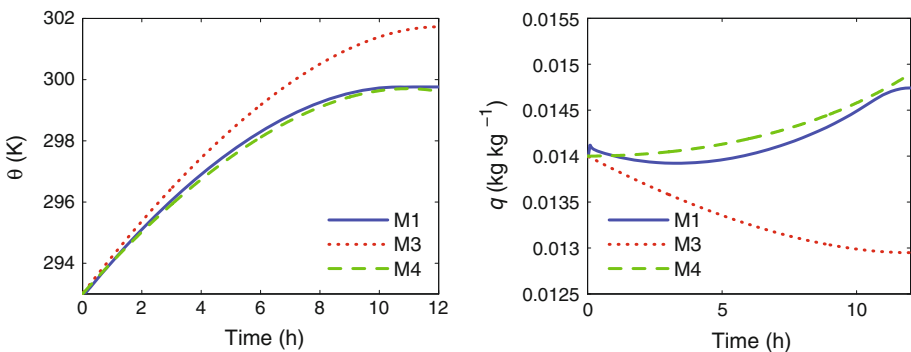


**Fig. 3** As in Fig. 2, but for potential temperature (left) and specific humidity (right)

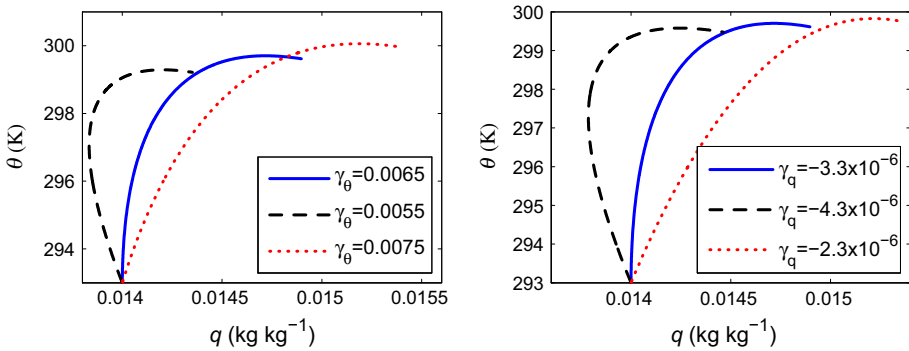


**Fig. 4** The diurnal mixing diagram resulting from the approximate analytical solution (other than specified in the legend, parameters are listed in Table 2)

As the potential temperature is a linear function of the ABL height (see Eq. 15), the approximate solution of potential temperature has the same shape as the approximate solution of  $h(t)$ . The fit with the specific humidity is not as close. Since the approximate solution was derived in part by linearizing the saturation vapour curve, it is perhaps no surprise that the resulting solution for the specific humidity is less perfect than that for  $h$  or  $\theta$ .

From Eqs. 15 and 16, the mixing diagram (Betts 1992) can be given analytically (inverting the axes) as

$$\tilde{q}(\tilde{\theta}) = \frac{\gamma_\theta(1 + \beta)}{\lambda\rho(1 + 2\beta)} \frac{1}{\tilde{\theta}} \int_0^{\tilde{\theta}} Q(u)du + \frac{1}{2}\tilde{\theta} \left( \frac{\gamma_q(1 + 2\beta)}{\gamma_\theta(1 + \beta)} - \frac{c_p}{\lambda(1 + \beta)} \right). \tag{34}$$

The resulting mixing diagram is shown in Fig. 4. Generally, humidity increases slower (or even decreases) in the morning and then increases more rapidly in the afternoon. This can be explained by the diurnal pattern of ABL growth rate that is more rapid in the morning and consistently decreases during the following day as shown in Fig. 1 (right). Due to this slowdown in ABL growth rate, entrainment from the free atmosphere transports more dry air into the ABL in the morning than in the afternoon, thus exhibiting a convex shape in the mixing diagram. When the potential temperature lapse rate ( $\gamma_\theta$ ) decreases, the atmosphere becomes more unstable and the ABL grows more rapidly, leading to greater dry air entrainment as shown in Fig. 4 (left). When increasing the slope of specific humidity ( $\gamma_q$ ), the atmosphere becomes more humid and entrainment brings more moist air to the ABL as indicated in Fig. 4 (right).

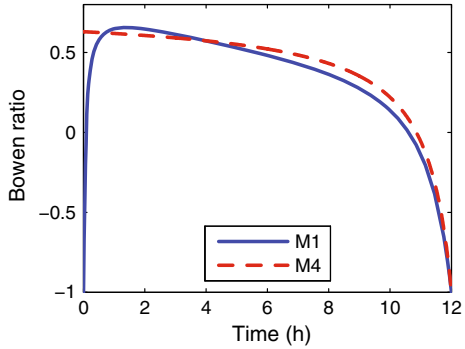
Instead of deriving the surface fluxes by directly analyzing the approximations of Eqs. 2a and 2b, it is simpler to use the approximate solution for the ABL height to derive the effective Bowen ratio. Using the approximated solution  $\bar{h}(t)$  in Eq. 33, its differential form  $\bar{h}'(t) = f(t)/h_{eq}(t) + C'$ , and ABL growth equation (8), one can obtain effective sensible heat flux ( $H_e(t)$ )

$$H_e(t) = \left[ \frac{f(t)}{h_{eq}(t)} + C' \right] [h_{eq}(t) + C't] \frac{\rho\gamma_\theta c_p}{1 + 2\beta}. \tag{35}$$

With Eq. 35, one can further find the effective Bowen ratio through the definition Eq. 12 as  $Bo_e(t) = H_e(t)/[Q(t) - H_e(t)]$ .

This Bowen ratio can then be used to find the surface sensible and latent heat fluxes in the same manner. The resulting Bowen ratio is shown in Fig. 5 with the numerical solution for

**Fig. 5** Bowen ratio from the full numerical simulation (M1) and analytical approximation (M4) (the parameters are listed in Table 2)



comparison. The approximate solution partitions heat flux well and, while simplifying the shape somewhat, also captures the time dependence of the Bowen ratio.

### 7 Solution with a Constant Effective Bowen Ratio (Model M5)

Porporato (2009) analytically solved a simplified case of constant Bowen ratio but left open the question of how to assign an appropriate value for the constant Bowen ratio. We have already shown that using the algebraic limit ( $Bo_{max} = Bo_{eq}$ ) derived in Porporato (2009) for the constant Bowen ratio corresponds to the equilibrium solution (28). However, this value is not the best choice for a constant effective Bowen ratio, since it would significantly overestimate the rate of growth of the mixed layer (see Fig. 1). A reasonable choice of constant effective Bowen ratio ( $Bo_{ce}$ ) is to use the mean value during the diurnal period,

$$Bo_{ce} = \frac{1}{T} \int_0^T Bo_e(u) du. \tag{36}$$

With the assumption of constant Bowen ratio  $Bo_{ce}$ ,  $\theta$  and  $q$  show a linear relationship with  $h$  as derived in Porporato (2009). Replacing the  $Bo$  in Eq. 13 with  $Bo_{ce}$ , one can find the governing equation for the boundary-layer growth,

$$\frac{dh}{dt} = \left( \frac{1 + 2\beta}{\rho c_p \gamma_\theta h} \right) \left[ \frac{Bo_{ce}}{1 + Bo_{ce}} Q(t) \right]. \tag{37}$$

This ordinary differential equation is solvable and the solutions to the ABL height and other atmospheric variables can be found in Porporato (2009), simply by replacing  $Bo$  with  $Bo_{ce}$ . This model is hereafter referred to as M5.

A comparison of the ABL height evolution from the full numerical simulation (M1) and this effective constant Bowen ratio model (M5) is shown in Fig. 6. As can be seen, the analytical solutions with effective constant Bowen ratio reach an acceptable approximation.

### 8 Model Testing

To test the various models and approximation methods (as listed in Table 1), we use sounding profiles and surface heat-flux data from the Atmospheric Radiation Measurement (ARM) Program (<http://www.arm.gov/>) at Central Facility in Southern Great Plains (CF-SGP).

**Fig. 6** The mixed-layer height predicted by the full numerical simulation (M1), constant equilibrium Bowen ratio (M3) and constant effective Bowen ratio (M5) (the parameters are listed in Table 2)

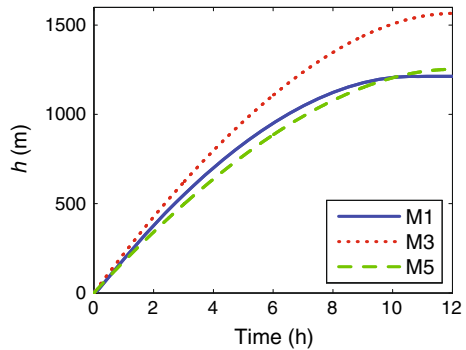


**Table 1** Summary of Hierarchy of Models

Model	Equation	Description
M0	–	Full numerical simulation of the coupled surface-ABL dynamics. The governing equations for M0 are the same as those for M1, except replacing $\theta$ , $\gamma_\theta$ , and $H$ with $\theta_v$ , $\gamma_{\theta_v}$ , and $H_v$ , respectively
M1	1–8	Full numerical simulation of the coupled surface-ABL dynamics ( $\overline{w'\theta'_v}$ is approximated as $\overline{w'\theta'}$ for parametrizing the entrainment flux)
M2	25	Numerical simulation of ABL dynamics with linearized saturation vapour pressure curve. The ABL height is modelled by Eq. 25. In this study, model M2 is a transitional model, which is then used to derive model M3, M4, and M5
M3	28	Analytical solutions for the ABL dynamics with assumption of constant equilibrium Bowen ratio
M4	33	Analytical approximation based on model M3 with further inclusion of $C'$ . ABL height [ $\bar{h}(t)$ ] is modeled in Eq. 33, and other ABL variables such as $\theta$ and $q$ can be derived by substituting $\bar{h}(t)$ for $h(t)$ in Eq. 15 and 16
M5	36	Analytical approximation for the ABL dynamics with the assumption of constant effective Bowen ratio

Radiosonde data in CF-SGP are often available in the early morning (0530 local time) and late afternoon (1730 local time). More details on radiosonde, surface flux and meteorological data can be found in Hubbe et al. (1997) and Santanello et al. (2005). Radiosonde measurements of temperature, pressure, and relative humidity were converted to profiles of potential temperature and specific humidity. Half-hour accumulated precipitation is available from the Surface Meteorological Observation System (SMOS). Half-hour averaged soil moisture, surface latent heat flux, and sensible heat flux are measured with an Energy Balance Bowen Ratio (EBBR) Station.

In CF-SGP, the vegetation is mainly grass and pasture. Under well-watered conditions, surface resistance  $r_s$  is set to a typical value of  $70 \text{ s m}^{-1}$ , and aerodynamic resistance  $r_a$  ( $\text{s m}^{-1}$ ) for the grass surface is approximated as  $r_a = 208/u_2$ , where  $u_2$  is the wind speed at 2 m (Allen et al. 1998). Net available energy is modelled as  $Q(t) = Q_{\max}[1 - (t/t_0 - 1)^2]$ , where  $t_0 = 6 \text{ h}$  is the time of midday.

Clear-sky days under well-watered conditions from 2002 to 2009 in summer were chosen to test the model. The calibrated parameters for these ensemble mean profiles (shown in

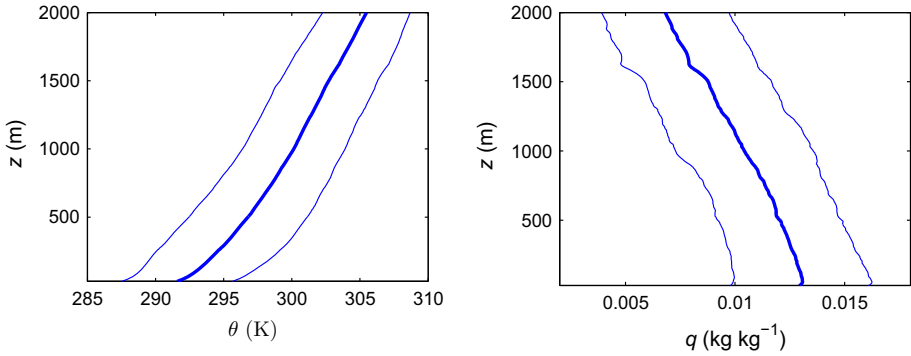


**Fig. 7** Ensemble profiles of early morning clear-sky potential temperature and specific humidity from 2002 to 2009 in summer under well-watered condition at the Central Facility, Southern Great Plain. The *thick line* shows the mean value, and the *solid lines* represent one standard deviation from the mean

**Table 2** Typical parameters for model testing derived from observations in CF-SGP

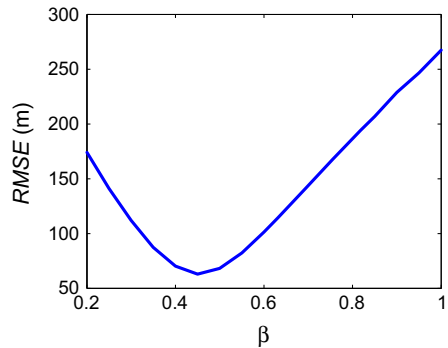
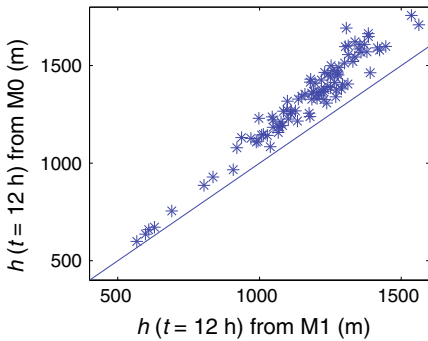
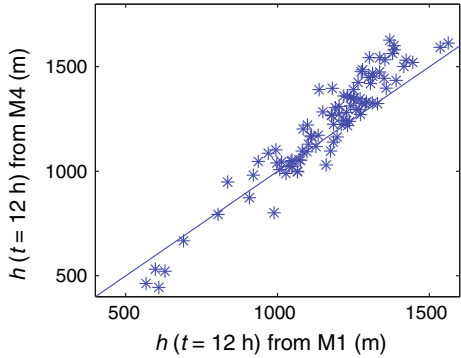
Variable	Value	Unit
$\beta$	0.2	–
$\lambda$	$2.45 \times 10^6$	$\text{J kg}^{-1}$
$\rho$	1.225	$\text{kg m}^{-3}$
$c_p$	1005	$\text{J kg}^{-1}\text{K}^{-1}$
$u_2$	5.44	$\text{m s}^{-1}$
$\gamma_\theta$	0.0065	$\text{K m}^{-1}$
$\theta_{f0}$	293	K
$\gamma_q$	$-3.3 \times 10^{-6}$	$\text{kg kg}^{-1}\text{m}^{-1}$
$q_{f0}$	0.014	$\text{kg kg}^{-1}$
$Q_{\max}$	493	$\text{W m}^{-2}$

Fig. 7), representing the typical atmospheric characteristics under well-watered conditions in the continental temperate region in summer, were used to test the various models and approximation methods as shown in Figs. 1, 2, 3, 4, 5 and 6. All these typical parameters are listed in Table 2.

To further test the approximation method from the linearized saturation curve and the inclusion of  $C'$  (M4), here we plot its solutions of ABL height at the end of the day against the full numerical simulations (M1) using the atmospheric parameters from the observations as in Fig. 8. As can be seen, the approximation method (M4) captures the essential ABL evolution under various climate conditions.

In the full numerical simulation model (M1), the sensible heat flux is used to approximate the buoyancy flux for the parametrization of the entrainment by neglecting humidity effects (i.e. the potential temperature is used in place of the virtual potential temperature). As noted by Driedonks (1982a), this approximation could underestimate the buoyancy flux and overestimate the strength of the buoyancy inversion, thus leading to slower ABL growth. To test this approximation, we plot the ABL height at the end of the day from the two numerical models with (M0) and without (M1) humidity effects using the same 94-day atmospheric parameters in Fig. 9 (left). As can be seen, the ABL height is slightly higher when humidity effects are considered (M0). However, since the errors are biased, it may be reasonable to

**Fig. 8** ABL height at the end of the day ( $t = 12$  h) predicted by analytical approximation M4 and full numerical simulation M1



**Fig. 9** *Left* ABL height at the end of the day predicted by the full numerical simulation M1 (without humidity effects on buoyancy) and M0 (with humidity effects on buoyancy). *Right* root-mean-square error (RMSE) of ABL height at the end of the day from M1 varying parameter  $\beta$

compensate part of these humidity effects by adjusting the entrainment ratio ( $\beta$ ). Figure 9 (right) shows that the root-mean-square error (RMSE) of the ABL at the end of the day can be reduced to a minimum value when the entrainment ratio  $\beta$  is around 0.45.

To analyze the sensitivity of certain parameters to Bowen ratio in the models, we control two important atmospheric characteristics ( $\gamma_\theta$  and  $\gamma_q$ ) and compare their sensitivity to the calculated constant effective Bowen ratio (M5) and the average daytime Bowen ratio from the full numerical simulation (M1) in Fig. 10. Generally, when the atmosphere is drier (smaller  $\gamma_q$ ), a higher vapour pressure deficit leads to greater evaporation and a lower Bowen ratio. When the upper atmosphere is colder (smaller  $\gamma_\theta$ ), the vapour pressure deficit may become relatively smaller during the growth of ABL, leading to less evaporation and higher Bowen ratios. Figure 10 also shows similar tendencies of the Bowen ratio for both models, indicating that it is possible to use the analytical approximation (M4) at least in the range specified here.

To demonstrate the detail of diurnal evolution of the ABL, we compare the daytime Bowen ratios from observation with the ones from full numerical simulation (M1), analytical approximation (M4), and constant effective Bowen ratio (M5) for two typical days at CF-SGP in Fig. 11. The numerical simulation and the approximation follow the diurnal variation of the observed Bowen ratios indicating the approximation can efficiently partition the sensible and the latent heat flux for the given available energy. The model M5 provides constant Bowen ratios for the heat-flux partitioning in the diurnal evolution and can be efficiently used to estimate the ABL growth as shown in Fig. 6.

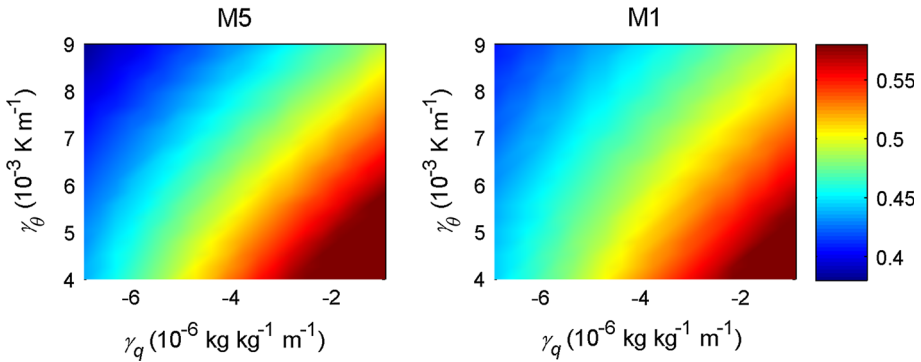


**Fig. 10** Sensitivity of  $\gamma_\theta$  and  $\gamma_q$  to the constant effective Bowen ratio (M5) and the average daytime Bowen ratio from the full numerical simulation (M1). The range of  $\gamma_\theta$  and  $\gamma_q$  covers the selected 94-day observations. Other parameters are typical values listed in Table 2

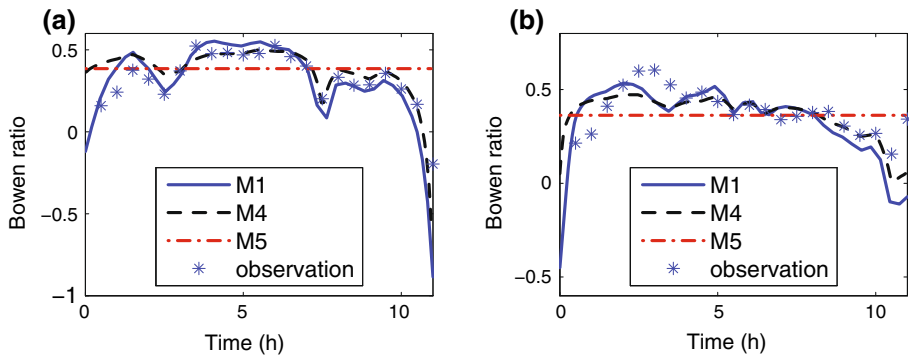


**Fig. 11** Diurnal evolution of Bowen ratio from the numerical simulation (M1), analytical approximation (M4), and observations on 22 June (a) and 25 June (b) 2007

### 9 Conclusions

We have presented a theoretical investigation of a mixed-layer model for the diurnal convective boundary layer dominated by buoyancy-drive turbulence for which the potential temperature and specific humidity can be solved in terms of the boundary-layer height and time. We have further derived the differential equation for the growth of the boundary layer,  $h(t)$ , in terms of  $h(t)$  and  $t$  only and shown, using perturbation methods, that the solution of Porporato (2009) assuming constant Bowen ratio represents the zero-order approximate solution to this differential equation. A closed form solution for the first-order approximation is derived here from which the entire system can be solved algebraically to first order for a given net radiation function  $Q(t)$ . The structure of the solution results from the two components of evaporation (i.e. equilibrium evaporation and evaporation due to the vapour pressure deficit), allowing us to see the effects of the energy and moisture balances on the growth of the ABL in closed form.

**Acknowledgments** We gratefully acknowledge funding from National Aeronautics and Space Administration (NASA grant NNX09AN76G), National Science Foundation (NSF-CBET-1033467, NSF-EAR-0838301, NSF-EAR-1331846, and NSF-EAR-1316258, NSF FESD 1338694), the US DOE through the Office of Bio-

logical and Environmental Research, Terrestrial Carbon Processes program (DE-SC0006967), as well as the Agriculture and Food Research Initiative from the USDA National Institute of Food and Agriculture (201167003-30222). Data were obtained from the Atmospheric Radiation Measurement Program sponsored by the U.S. Department of Energy. The comments and useful criticisms of anonymous reviewers are gratefully acknowledged.

## References

- Allen RG, Pereira LS, Raes D, Smith M et al (1998) Crop evapotranspiration-Guidelines for computing crop water requirements-FAO Irrigation and drainage paper 56. Food and Agriculture Organization of the United Nations, Rome, 300 pp
- Angevine W (2008) Transitional, entraining, cloudy, and coastal boundary layers. *Acta Geophys* 56(1):2–20
- Ball F (1960) Control of inversion height by surface heating. *Q J R Meteorol Soc* 86(370):483–494
- Batchvarova E, Gryning SE (1991) Applied model for the growth of the daytime mixed layer. *Boundary-Layer Meteorol* 56(3):261–274
- Batchvarova E, Gryning SE (1994) An applied model for the height of the daytime mixed layer and the entrainment zone. *Boundary-Layer Meteorol* 71(3):311–323
- Betts A (1973) Non-precipitating cumulus convection and its parameterization. *Q J R Meteorol Soc* 99(419):178–196
- Betts A (1992) Fife atmospheric boundary layer budget methods. *J Geophys Res Atmos* 97(D17):18,523–18,531
- Betts AK (1994) Relation between equilibrium evaporation and the saturation pressure budget. *Boundary-Layer Meteorol* 71(3):235–245
- Brutsaert W (1987) Nearly steady convection and the boundary-layer budgets of water vapor and sensible heat. *Boundary-Layer Meteorol* 39(3):283–300
- Brutsaert W (2005) *Hydrology: an introduction*. Cambridge University Press, New York, 605 pp
- Canut G, Couvreur F, Lothon M, Pino D, Said F (2012) Observations and large-eddy simulations of entrainment in the sheared sahelian boundary layer. *Boundary-Layer Meteorol* 142(1):79–101
- Carson D (1973) The development of a dry inversion-capped convectively unstable boundary layer. *Q J R Meteorol Soc* 99(421):450–467
- Culf AD (1994) Equilibrium evaporation beneath a growing convective boundary layer. *Boundary-Layer Meteorol* 70(1–2):37–49
- De Bruin H (1983) A model for the priestley-taylor parameter  $\alpha$ . *J Clim Appl Meteorol* 22(4):572–578
- Driedonks A (1982a) Models and observations of the growth of the atmospheric boundary layer. *Boundary-Layer Meteorol* 23(3):283–306
- Driedonks A (1982b) Sensitivity analysis of the equations for a convective mixed layer. *Boundary-Layer Meteorol* 22(4):475–480
- Garratt JR (1994) *The atmospheric boundary layer*. Cambridge University Press, Cambridge, 316 pp
- Hubbe J, Doran J, Liljegren J, Shaw W (1997) Observations of spatial variations of boundary layer structure over the southern great plains cloud and radiation testbed. *J Appl Meteorol* 36(9):1221–1231
- Juang JY, Porporato A, Stoy PC, Siqueira MS, Oishi AC, Detto M, Kim HS, Katul GG (2007) Hydrologic and atmospheric controls on initiation of convective precipitation events. *Water Resour Res* 43(3):W03,421
- Kim C, Entekhabi D (1998) Feedbacks in the land-surface and mixed-layer energy budgets. *Boundary-Layer Meteorol* 88(1):1–21
- Konings AG, Katul GG, Porporato A (2010) The rainfall-no rainfall transition in a coupled land-convective atmosphere system. *Geophys Res Lett* 37(14):L14,401
- Lilly D (1968) Models of cloud-topped mixed layers under a strong inversion. *Q J R Meteorol Soc* 94(401):292–309
- Logan JD (2013) *Applied mathematics*. Wiley, Hoboken, 658 pp
- Lyons T (2002) Clouds prefer native vegetation. *Meteorol Atmos Phys* 80(1–4):131–140
- Mahrt L (1976) Mixed layer moisture structure. *Mon Weather Rev* 104(11):1403–1407
- McNaughton K (1976) Evaporation and advection I: evaporation from extensive homogeneous surfaces. *Q J R Meteorol Soc* 102(431):181–191
- McNaughton K, Spriggs T (1986) A mixed-layer model for regional evaporation. *Boundary-Layer Meteorol* 34(3):243–262
- Pelly J, Belcher S (2001) A mixed-layer model of the well-mixed stratocumulus-topped boundary layer. *Boundary-Layer Meteorol* 100(1):171–187

- Porporato A (2009) Atmospheric boundary-layer dynamics with constant Bowen ratio. *Boundary-Layer Meteorol* 132(2):227–240
- Priestley C, Taylor R (1972) On the assessment of surface heat flux and evaporation using large-scale parameters. *Mon Weather Rev* 100(2):81–92
- Raupach M (1998) Radiative physiological, aerodynamic and boundary-layer feedbacks on the terrestrial surface energy balance. *Glob Change Biol* 4:477–494
- Raupach M (2000) Equilibrium evaporation and the convective boundary layer. *Boundary-Layer Meteorol* 96(1–2):107–142
- Raupach M (2001) Combination theory and equilibrium evaporation. *Q J R Meteorol Soc* 127(574):1149–1181
- Santanello JA, Friedl MA, Kustas WP (2005) An empirical investigation of convective planetary boundary layer evolution and its relationship with the land surface. *J Appl Meteorol* 44(6):917–932
- Seibert P, Beyrich F, Gryning SE, Joffre S, Rasmussen A, Tercier P (2000) Review and intercomparison of operational methods for the determination of the mixing height. *Atmos Environ* 34(7):1001–1027
- Siqueira M, Katul G, Porporato A (2009) Soil moisture feedbacks on convection triggers: the role of soil–plant hydrodynamics. *J Hydrometeorol* 10(1):96–112
- Stull RB (1976) The energetics of entrainment across a density interface. *J Atmos Sci* 33(7):1260–1267
- Stull RB (1988) *An introduction to boundary layer meteorology*. Kluwer, Dordrecht, 666 pp
- Tennekes H (1973) A model for the dynamics of the inversion above a convective boundary layer. *J Atmos Sci* 30(4):558–567
- Van Heerwaarden CC, Vilà-Guerau de Arellano J, Moene AF, Holtslag AA (2009) Interactions between dry-air entrainment, surface evaporation and convective boundary-layer development. *Q J R Meteorol Soc* 135(642):1277–1291
- Zaitsev VF, Polyanin AD (2012) *Handbook of exact solutions for ordinary differential equations*. CRC Press, Boca Raton, 791 pp